

Confined Coulomb systems with adsorbing boundaries: the two-dimensional two-component plasma

Lina Merchán* and Gabriel Téllez†

Departamento de Física, Universidad de Los Andes, A.A. 4976, Bogotá, Colombia

Using a solvable model, the two-dimensional two-component plasma, we study a Coulomb gas confined in a disk and in an annulus with boundaries that can adsorb some of the negative particles of the system. We obtain explicit analytic expressions for the grand potential, the pressure and the density profiles of the system. By studying the behavior of the disjoining pressure we find that without the adsorbing boundaries the system is naturally unstable, while with attractive boundaries the system is stable because of a positive contribution from the surface tension to the disjoining pressure. The results for the density profiles show the formation of a positive layer near the boundary that screens the adsorbed negative particles, a typical behavior in charged systems. We also compute the adsorbed charge on the boundary and show that it satisfies a certain number of relations, in particular an electro-neutrality sum rule.

Keywords: Coulomb systems, two-component plasma, adsorbing boundaries, soap films and bubbles, micelles and vesicles, disjoining pressure, charge density

I. INTRODUCTION

In this paper we study the classical (i.e. non-quantum) equilibrium statistical mechanic properties of confined Coulomb systems with adsorbing boundaries. A Coulomb system is a system of charged particles interacting through the Coulomb potential. There are several interesting realizations of Coulomb systems with several applications such as plasmas, electrolytes, colloidal suspensions, etc... In the present paper we are interested in the case where the Coulomb system is confined with boundaries that can attract and adsorb some particles of the system. Our study of this kind of systems will be done using a solvable model of Coulomb system: the symmetric two-dimensional two-component plasma, a system of two kind of oppositely charged particles $\pm q$ at thermal equilibrium at an inverse temperature $\beta = (k_B T)^{-1}$. The classical equilibrium statistical mechanics of the system can be exactly solved when $\beta q^2 = 2$.

One can think of several examples where the present situation of Coulomb systems confined with adsorbing boundaries is relevant, for instance in a plasma or an electrolyte near an electrode with adsorbing sites [1, 2]. Another situation in which we will focus our attention is in solutions of amphiphathic molecules and ions for example in soap films and bubbles. Amphiphathic molecules have an hydrophobic tail and an hydrophilic charged head (usually negative) and, for this reason, when they are submerged in water they rearrange themselves in such a way as to minimize the contact of the hydrophobic tails with the surrounding medium. They can achieve configurations such as bilayers, micelles and vesicles, among others.

In a previous paper [3] we studied a soap film by model-

ing it as a Coulomb system confined in a slab. A soap film can be seen as a system of amphiphathic molecules in a bilayer configuration with a water inner layer. The overall neutral system with negatively charged amphiphathic anions and positive micro-cations (usually Na^+) in water was modeled as a two-dimensional two-component plasma. The two dimensions were in the breadth of the film not on the surface: we studied a cross section of the film. Because of the hydrophobicity of their tails, the soap anions prefer to be in the boundaries of the film. This was modeled by a one-body attractive short-range external potential acting over them. This means that the negative particles felt an attractive potential over a small distance near each boundary. In this sense the negative particles of the system can be “adsorbed” by the boundary.

In Ref. [3] we found exact expressions for the density, correlations and pressure inside the film. By studying the disjoining pressure, we were able to conclude that the Coulomb interaction plays an important role in the collapse of a thick soap film to a much thinner film. Actually if a large number of amphiphathic molecules are in the boundary due to a large strength of the attractive external potential near the boundary, the system is always stable. On the other hand if the attractive potential near the boundary is not strong enough a thick film will not be stable and will collapse to a thin film.

These results can be compared (qualitatively due to the simplicity of the model under consideration) to the experimental situation of the transition of a thick film to a thin black film. These black film phenomena occur when the soap films width is smaller than visible light wavelength and it is seen black. Two types of black films are observed experimentally: the common black film and the much thinner Newton black film.

It is interesting to know to what extent the results of our previous work [3] depend on the geometry. Here we study this two-component plasma system confined in two other geometries, a disk and an annulus. As

*Electronic address: l-mercha@uniandes.edu.co

†Electronic address: gtellez@uniandes.edu.co

we mentioned before, amphiphathic molecules in water can achieve micelles and vesicles among others configurations. In two dimensions, a cylindrical micelle can be seen as a disk and a cylindrical vesicle as an annulus. If the length of the cylindrical micelle or vesicle is much larger than its radius it is reasonable to assume that the system is invariant in the longitudinal direction and so we study only a cross section of the system: a disk or an annulus. The Coulomb interaction is then the two-dimensional Coulomb potential which is $v_c(r) = -\ln(r/d)$ for two particles at a distance r of each other. The length d is an arbitrary length which fixes the zero of the potential.

Two-dimensional Coulomb systems with log interaction have properties that are similar to those in three dimensional charged systems with the usual $1/r$ potential. They satisfy Gauss law and Poisson equation in two dimensions. Several universal properties, such as screening effects, are direct consequences of the harmonic nature of the $-\ln(r/d)$ and $1/r$ potentials, which are the solutions of the two- and three-dimensional Poisson equation. Therefore the exact solutions obtained for the 2D models play an important role in understanding real 3D Coulomb systems.

The rest of this work is organized as follows. In section II we present in detail the system under consideration and briefly review how this model can be exactly solved. In section III we compute the grand potential of the system and the disjoining pressure and study the stability of the system. In section IV we compute the density profiles of the different types of particles in the system and the adsorbed charge on the boundaries. Finally, we conclude recalling the main results of the present work.

II. THE MODEL AND METHOD OF SOLUTION

The system under consideration is a two-dimensional system composed of two types of point particles with charges $\pm q$. Two particles with charges sq and $s'q$ at a distance r apart interact with the two-dimensional Coulomb potential $-ss'q^2 \ln(r/d)$ where d is an arbitrary length. This system is known as the symmetric two-dimensional two-component plasma.

When the Boltzmann factor for the Coulomb potential is written, the adimensional coulombic coupling constant appears: $\Gamma = q^2/k_B T = \beta q^2$. Notice that in two dimensions q^2 has dimensions of energy. For a system of point particles if $\Gamma \geq 2$ the system is unstable against the collapse of particles of opposite sign, the thermodynamics of the system are not well defined unless one considers hard-core particles or another regularization procedure (for instance a lattice model instead of a continuous gas). On the other hand, if $\Gamma < 2$ the thermal agitation is enough to avoid the collapse and the system of point particles is well defined. The two-component plasma is known to be equivalent to the sine-Gordon model and using this relationship and the results known for this in-

tegrable field theory, the thermodynamic properties of the two-component plasma in the bulk have been exactly determined [4] in the whole range of stability $\Gamma < 2$. However, there are no exact results for confined systems for arbitrary Γ (with the exception of a Coulomb system near an infinite plane conductor [5] or ideal dielectric [6] wall).

It is also well-known for some time that when $\Gamma = 2$ the sine-Gordon field theory is at its free fermion point. This means that the system is equivalent to a free fermion field theory and therefore much more information on the system can be obtained. In particular the thermodynamic properties and correlation functions can be exactly computed even for confined systems in several different geometries and different boundary conditions [7, 8, 9, 10, 11, 12, 13, 14]. From now on we will consider only the case when $\Gamma = 2$.

Since at $\Gamma = 2$ a system of point particles is not stable one should start with a regularized model with a cutoff distance a which can be the diameter of the hard-core particles or the lattice spacing in a lattice model [7]. The system is worked out in the grand-canonical ensemble at given chemical potentials μ_+ and μ_- for the positive and negative particles respectively. In the limit of a continuous model $a \rightarrow 0$ the grand partition function and the bulk densities diverge. However the correlation functions have a well-defined limit. In this continuous limit it is useful to work with the rescaled fugacities [9] $m_{\pm} = 2\pi d e^{\beta\mu_{\pm}}/a^2$ that have inverse length dimensions. The length m^{-1} can be shown to be the screening length of the system [9]. If external potentials $V_{\pm}(\mathbf{r})$ act on the particles (as in our case) it is useful to define position dependent fugacities $m_{\pm}(\mathbf{r}) = m_{\pm} \exp(-\beta V_{\pm}(\mathbf{r}))$.

Let us briefly review the method of resolution described by Cornu and Jancovici [8, 9] for the two-component plasma. It will be useful to use the complex coordinates $z = r e^{i\theta} = x + iy$ for the position of the particles. For a continuous model, $a \rightarrow 0$, ignoring the possible divergences for the time being, it is shown in Ref. [9] that the equivalence of the two-component plasma with a free fermion theory allows the grand partition function to be written as

$$\Xi = \det \left[\begin{pmatrix} 0 & 2\partial_z \\ 2\partial_{\bar{z}} & 0 \end{pmatrix}^{-1} \begin{pmatrix} m_+(\mathbf{r}) & 2\partial_z \\ 2\partial_{\bar{z}} & m_-(\mathbf{r}) \end{pmatrix} \right] \quad (2.1)$$

Then defining an operator K as

$$K = \begin{pmatrix} 0 & 2\partial_z \\ 2\partial_{\bar{z}} & 0 \end{pmatrix}^{-1} \begin{pmatrix} m_+(\mathbf{r}) & 0 \\ 0 & m_-(\mathbf{r}) \end{pmatrix} \quad (2.2)$$

the grand partition function Ξ can be expressed as

$$\Xi = \det(1 + K). \quad (2.3)$$

The calculation of the grand potential $\beta\Omega = -\ln \Xi$ and the pressure $p = -\partial\Omega/\partial V$ where V is the volume (in a two-dimensional system this refers to the area), reduces

to finding the eigenvalues of K because the grand potential can be written as

$$\Omega = -k_B T \sum_i \ln(1 + \lambda_i) \quad (2.4)$$

where λ_i are the eigenvalues of the operator K .

On the other hand, the calculation of the one-particle densities and correlations reduces to finding a special set of Green functions. As usual, the density can be expressed as a functional derivative

$$\rho_{\pm}(r) = m_{\pm}(r) \frac{\delta \ln \Xi}{\delta m_{\pm}(r)} \quad (2.5)$$

If we define the 2×2 matrix

$$\mathbf{G}(\mathbf{r}_1, \mathbf{r}_2) = \begin{pmatrix} G_{++}(\mathbf{r}_1, \mathbf{r}_2) & G_{+-}(\mathbf{r}_1, \mathbf{r}_2) \\ G_{-+}(\mathbf{r}_1, \mathbf{r}_2) & G_{--}(\mathbf{r}_1, \mathbf{r}_2) \end{pmatrix} \quad (2.6)$$

as the kernel of the inverse of the operator

$$\begin{pmatrix} m_+(\mathbf{r}) & 2\partial_z \\ 2\partial_{\bar{z}} & m_-(\mathbf{r}) \end{pmatrix} \quad (2.7)$$

then the one-body density and two-body Ursell functions can be expressed in terms of these Green functions as

$$\begin{aligned} \rho_{s_1}(\mathbf{r}_1) &= m_{s_1} G_{s_1 s_1}(\mathbf{r}_1, \mathbf{r}_1), \\ \rho_{s_1 s_2}^{(2)T}(\mathbf{r}_1, \mathbf{r}_2) &= -m_{s_1} m_{s_2} G_{s_1 s_2}(\mathbf{r}_1, \mathbf{r}_2) G_{s_2 s_1}(\mathbf{r}_2, \mathbf{r}_1) \end{aligned} \quad (2.8)$$

where $s_{1,2} \in \{+, -\}$ denote the sign of the particles. In polar coordinates these Green functions satisfy the following set of equations

$$\begin{bmatrix} m_+(\mathbf{r}_1) & e^{-i\theta_1} \left[\partial_{r_1} - \frac{i\partial_{\theta_1}}{r_1} \right] \\ e^{i\theta_1} \left[\partial_{r_1} + \frac{i\partial_{\theta_1}}{r_1} \right] & m_-(\mathbf{r}_1) \end{bmatrix} \mathbf{G} = \delta(\mathbf{r}_1 - \mathbf{r}_2) \mathbb{I} \quad (2.9)$$

with \mathbb{I} being the unit 2×2 matrix.

The above formalism is very general, it can be applied to a variety of situations. In the case we are interested in, we will consider two geometries in which the system is confined: a disk of radius R and an annulus of inner and outer radius R_1 and R_2 respectively.

The negative particles are supposed to model amphiphathic molecules and therefore they are attracted to the boundaries of the system while positive particles are not. This is modeled by an attractive external one-body potential $V_-(\mathbf{r})$ acting on the negative particles near the boundary while for the positive particles $V_+(\mathbf{r}) = 0$.

Actually we will consider two models for this potential. In the first model (model I) the fugacity $m_-(\mathbf{r})$ for the negative particles reads, for the disk geometry,

$$m_-(\mathbf{r}) = m e^{-\beta V_-(\mathbf{r})} = m + \alpha \delta(r - R) \quad (2.10)$$

inside the disk, while $m_+ = m$ is constant. Outside the disk $r > R_2$ both fugacities vanish. In the annulus geometry,

$$m_-(\mathbf{r}) = m + \alpha_1 \delta(r - R_1) + \alpha_2 \delta(r - R_2) \quad (2.11)$$

inside the annulus. The coefficients α , α_1 and α_2 measure the strength of the attraction to the walls. In the following we will call these coefficients adhesivities.

In the second model (model II) that we will eventually consider the external potential $V_-(\mathbf{r})$ is a step function with a range $\tilde{\delta}$ of attraction near the boundary. This model allows us to obtain valuable information regarding the frontier regions. Actually we will report here only the main results for the annulus geometry with model II in section IV C, further results on this model on the disk geometry can be found in Ref. [15].

In the two following sections we will apply the method presented here to obtain the grand potential and the density profiles of the system.

III. THE PRESSURE

A. The grand potential

To find the pressure of the confined Coulomb system we proceed first to compute the grand potential. As shown in section II the grand potential Ω is given by

$$\beta \Omega = -\ln \prod_i (1 + \lambda_i) \quad (3.1)$$

where λ_i are the eigenvalues of the operator K given by equation (2.2). The eigenvalue problem for K with eigenvalue λ and eigenvector (ψ, χ) reads

$$m_-(\mathbf{r})\chi(\mathbf{r}) = 2\lambda\partial_z\psi(\mathbf{r}) \quad (3.2a)$$

$$m_+(\mathbf{r})\psi(\mathbf{r}) = 2\lambda\partial_z\chi(\mathbf{r}) \quad (3.2b)$$

These two equations can be combined into

$$\Delta\chi(\mathbf{r}) = \frac{m_+(\mathbf{r})m_-(\mathbf{r})}{\lambda^2} \chi(\mathbf{r}) \quad (3.3)$$

We now detail the computation of the grand potential for the case of a Coulomb system confined in a disk. The annulus geometry follows similar calculations.

We will only use model I for the attracting potential on the boundary for the calculation of the grand potential. Using model I the fugacities inside the disk read

$$m_+(\mathbf{r}) = m, \quad m_-(\mathbf{r}) = m + \alpha\delta(r - R), \quad (3.4)$$

and outside the disk they vanish. Replacing these fugacities into the eigenvalue problem equations (3.2) we find that $\chi(\mathbf{r})$ is a continuous function while $\psi(\mathbf{r})$ is discontinuous at $r = R$ due to the Dirac delta distribution in $m_-(\mathbf{r})$. The discontinuity of ψ is given by

$$\psi(R^+, \theta) - \psi(R^-, \theta) = \frac{\alpha}{\lambda} \chi(R, \theta) e^{-i\theta} \quad (3.5)$$

Defining $k = m/\lambda$, inside the disk $r < R$, $\chi(\mathbf{r})$ obeys the equation

$$\Delta\chi(\mathbf{r}) = k^2\chi(\mathbf{r}) \quad (3.6)$$

with solutions of the form

$$\chi(r, \theta) = A_l e^{il\theta} I_l(kr) \quad (3.7)$$

and

$$\psi(r, \theta) = A_l e^{i(l-1)\theta} I_{l-1}(kr) \quad (3.8)$$

where I_l is a modified Bessel function of order l . Outside the disk $m_- = m_+ = 0$ and the corresponding solutions to equations (3.2) are that ψ is analytic and χ anti-analytic, namely,

$$\chi(\mathbf{r}) = B_l e^{il\theta} r^{-l} \quad (3.9)$$

$$\psi(\mathbf{r}) = B_l e^{i(l-1)\theta} r^{l-1}. \quad (3.10)$$

In order to have vanishing solutions at $r \rightarrow \infty$ it is necessary that

$$\psi(R^+, \theta) = 0, \quad \text{if } l \geq 1 \quad (3.11a)$$

$$\chi(R, \theta) = 0, \quad \text{if } l \leq 0 \quad (3.11b)$$

Using these boundary conditions together with the continuity of χ at R and the discontinuity (3.5) of ψ at R gives the eigenvalue equation

$$I_l\left(\frac{mR}{\lambda}\right) = 0 \quad \text{if } l \leq 0 \quad (3.12a)$$

$$\alpha I_l\left(\frac{mR}{\lambda}\right) + I_{l-1}\left(\frac{mR}{\lambda}\right) = 0 \quad \text{if } l \geq 1 \quad (3.12b)$$

The product appearing in equation (3.1) can be partially computed by recognizing that the l.h.s of the eigenvalue equation (3.12) for arbitrary λ can be written as a Weierstrass product [3, 12, 14, 16]. Let us introduce the analytic functions

$$f_l^{(-)}(z) = I_l(mzR) l! \left(\frac{2}{mzR}\right)^l \quad (3.13)$$

$$f_l^{(+)}(z) = [\alpha I_l(mzR) + I_{l-1}(mzR)] (l-1)! \left(\frac{2}{mzR}\right)^{l-1} \quad (3.14)$$

By construction the zeros of $f_l^{(+)}$ are the inverse of the eigenvalues λ for $l > 0$ and the zeros of $f_{-l}^{(-)}$ are the inverse eigenvalues λ for $l \leq 0$. Furthermore, since $f_l^{(\pm)}(0) = 1$, $f_l^{(\pm)}(0) = 0$ and $f_l^{(\pm)}(z)$ is an even function it can be factorized as the Weierstrass product

$$f_l^{(\pm)}(z) = \prod_{\lambda_l} \left(1 - \frac{z}{\lambda_l^{-1}}\right) \quad (3.15)$$

where the product runs over all λ_l solutions of equation (3.12) for a given l . Then we can conclude that the grand potential (3.1) is given by

$$\beta\Omega = \sum_{l=0}^{\infty} \ln f_l^{(-)}(-1) + \sum_{l=1}^{\infty} \ln f_l^{(+)}(-1) \quad (3.16)$$

After shifting by one the index in the second sum and rearranging the expression we find the final result for the grand potential

$$\Omega^D = \Omega_{\text{hw}}^D + \Omega_{\text{at}}^D \quad (3.17)$$

with

$$\beta\Omega_{\text{hw}}^D = -2 \sum_{l=0}^{\infty} \ln \left[l! \left(\frac{2}{mR}\right)^l I_l(mR) \right] \quad (3.18)$$

which is the grand potential for a two-component plasma in a disk with hard wall boundaries [11] ($\alpha = 0$) and

$$\beta\Omega_{\text{at}}^D = - \sum_{l=0}^{\infty} \ln \left[1 + \alpha \frac{I_{l+1}(mR)}{I_l(mR)} \right] \quad (3.19)$$

is the contribution due to the attractive potential near the walls.

Now we turn our attention to the case of the Coulomb system confined in an annulus of inner radius R_1 and outer radius R_2 . In this case the position-dependent fugacity for the negative particles inside the annulus is given by

$$m_-(\mathbf{r}) = m + \alpha_1 \delta(r - R_1) + \alpha_2 \delta(r - R_2) \quad (3.20)$$

The calculation of the grand potential follows similar steps as above. One should solve the Laplacian eigenvalue problem with the appropriate boundary conditions given by the continuity of χ and the discontinuity of ψ at R_1 and R_2 . After some straightforward calculations the final result for the grand potential is

$$\Omega^A = \Omega_{\text{hw}}^A + \Omega_{\text{at}}^A \quad (3.21)$$

with

$$\beta\Omega_{\text{hw}}^A = -2 \sum_{l=0}^{\infty} \ln \left[\frac{mR_1^{l+1}}{R_2^l} (I_l(mR_2)K_{l+1}(mR_1) + I_{l+1}(mR_1)K_l(mR_2)) \right] \quad (3.22)$$

and

$$\beta\Omega_{\text{at}}^{\text{A}} = -\sum_{l=0}^{\infty} \ln \left[1 + \alpha_1 \frac{I_l(mR_2)K_l(mR_1) - K_l(mR_2)I_l(mR_1)}{I_l(mR_2)K_{l+1}(mR_1) + I_{l+1}(mR_1)K_l(mR_2)} \right] - \sum_{l=0}^{\infty} \ln \left[1 + \alpha_2 \frac{I_{l+1}(mR_2)K_{l+1}(mR_1) - K_{l+1}(mR_2)I_{l+1}(mR_1)}{I_l(mR_2)K_{l+1}(mR_1) + I_{l+1}(mR_1)K_l(mR_2)} \right] \quad (3.23)$$

The first term $\Omega_{\text{hw}}^{\text{A}}$ is the grand potential for a two-dimensional two-component plasma confined in an annulus [11] with hard wall boundaries¹ ($\alpha = 0$) and the second term $\Omega_{\text{at}}^{\text{A}}$ is the contribution to the grand potential due to the attractive nature of the walls.

It should be noted that all sums (3.18), (3.19), (3.22) and (3.23) above are divergent and should be cutoff to obtain finite results. This is due to the fact that the two-component plasma of point particles is not stable against the collapse of particles of opposite sign for $\beta q^2 \geq 2$ and a short-distance cutoff a should be introduced, a can be interpreted as the hard-core diameter of the particles. If R is the characteristic size of the system (for instance the radius of the disk in the disk case) then l/R is a wavelength and the short-distance cutoff a gives an ultraviolet cutoff $1/a$. Then the cutoff for l (say N) in the sums should be chosen of order R/a [9, 11].

B. Finite-size corrections

It is instructive to study the behavior of the grand potential when the system is large. It has been known for some time that two-dimensional Coulomb systems in their conducting phase have a similar behavior to critical systems [11, 12]. In particular the grand potential of a two-dimensional Coulomb system confined in a domain of characteristic size L has a large- L expansion

$$\beta\Omega = AL^2 + BL + \frac{\chi}{6} \ln L + O(1) \quad (3.24)$$

similar to the one predicted by Cardy [17, 18] for critical systems. The first two terms are respectively the bulk grand potential and the surface contribution to the grand potential (the surface tension) and are non-universal. The logarithmic term is a universal finite-size correction to the grand potential, it does not depend on the microscopic detail of the system, only on the topology of the manifold where the system lives through the Euler characteristic χ . For a disk $\chi = 1$ and for an annulus $\chi = 0$.

It is interesting to verify if this finite-size expansion holds for the systems studied here, in particular if the finite-size correction is modified by the special attractive nature of the walls considered here.

Let us first consider the case of the disk geometry. We choose to cutoff the sums (3.18) and (3.19) to a maximum value for l equal to R/a and the results given here are for $a \rightarrow 0$. The finite-size expansion for large- R of the hard wall contribution to the grand potential has already been computed in Ref. [11] with the result

$$\beta\Omega_{\text{hw}}^{\text{D}} = -\beta p_b \pi R^2 + \beta \gamma_{\text{hw}} 2\pi R + \frac{1}{6} \ln(mR) + O(1) \quad (3.25)$$

where the bulk pressure p_b is given by

$$\beta p_b = \frac{m^2}{2\pi} \left(1 + \ln \frac{2}{ma} \right) \quad (3.26)$$

and the surface tension γ_{hw} for hard walls is given by

$$\beta \gamma_{\text{hw}} = m \left(\frac{1}{4} - \frac{1}{2\pi} \right) \quad (3.27)$$

We only need to compute the large- R expansion of (3.19). This can be done expressing the Bessel function $I_{l+1}(mR)$ as $I_{l+1}(mR) = I'_l(mR) + lI_l(mR)/(mR)$, using the uniform Debye expansions [19] of the Bessel functions valid for large argument

$$I_l(z) \sim \frac{e^\eta}{\sqrt{2\pi}(l^2 + z^2)^{1/4}} \left[1 + \frac{3t - 5t^3}{24l} + \dots \right] \quad (3.28a)$$

$$I'_l(z) \sim \frac{(l^2 + z^2)^{1/4} e^\eta}{\sqrt{2\pi} z} \left[1 - \frac{9t - 7t^3}{24l} + \dots \right] \quad (3.28b)$$

with $\eta = \sqrt{l^2 + z^2} + l \ln \left(\frac{z}{l + \sqrt{l^2 + z^2}} \right)$ and $t = l/\sqrt{l^2 + z^2}$, and using the Euler-McLaurin formula to transform the summation into an integral

$$\sum_{l=0}^N f(l) = \int_0^N f(x) dx + \frac{1}{2} [f(N) + f(0)] + \frac{1}{12} [f'(N) - f'(0)] + \dots \quad (3.29)$$

After some calculations, taking first the limit $N \rightarrow \infty$, keeping only the non-vanishing terms, then taking the limit $R \rightarrow \infty$ and replacing N by R/a , we find that (3.19)

¹ Eq. (4.16) of Ref. [11] for the grand potential in an annulus with hard wall boundaries is incorrect, however the equation above (4.16) is correct and gives our result (3.22) for the grand potential

contributes only to the surface tension giving for the grand potential the final result

$$\beta\Omega^D = -\beta p_b \pi R^2 + 2\pi R \beta\gamma + \frac{1}{6} \ln(mR) + O(1) \quad (3.30)$$

where the surface tension is now given by

$$\beta\gamma = -\frac{m}{4\pi} \left[\alpha \ln \frac{2}{ma} + 1 - \pi + \alpha + \frac{1 - \alpha^2}{\alpha} \ln(\alpha + 1) \right] \quad (3.31)$$

We recover as expected the surface tension obtained in Ref. [3] for the same system but confined in a slab.

The universal logarithmic finite-size correction $(1/6) \ln(mR)$ is still present and it is not modified by the presence of the attractive boundaries.

For the annulus geometry we are interested in the limit $R_1 \rightarrow \infty$ and $R_2 \rightarrow \infty$ with R_2/R_1 finite. We proceed as above, using also this time the Debye expansion for the Bessel functions [19]

$$K_l(z) \sim \frac{\sqrt{\pi} e^{-\eta}}{\sqrt{2}(l^2 + z^2)^{1/4}} \left[1 - \frac{3t - 5t^3}{24l} + \dots \right] \quad (3.32a)$$

$$K'_l(z) \sim \frac{-\sqrt{\pi}(l^2 + z^2)^{1/4} e^{-\eta}}{\sqrt{2}z} \left[1 + \frac{9t - 7t^3}{24l} + \dots \right] \quad (3.32b)$$

Using (3.28) and (3.32) one can notice that inside the logarithm in (3.22) the term $I_{l+1}(mR_1)K_l(mR_2)$ is exponentially small compared to $I_l(mR_2)K_{l+1}(mR_1)$ since $R_2 - R_1 \rightarrow \infty$. Also in the contribution from the attractive boundaries (3.23) the dominant terms are

$$\beta\Omega_{\text{at}}^A \sim -\sum_{l=0}^N \ln \left[1 + \alpha_1 \frac{K_l(mR_1)}{K_{l+1}(mR_1)} \right] - \sum_{l=0}^N \ln \left[1 + \alpha_2 \frac{I_{l+1}(mR_2)}{I_l(mR_2)} \right] \quad (3.33)$$

Then, after some calculations we get the final result

$$\beta\Omega^A = -\beta p_b \pi (R_2^2 - R_1^2) + \beta\gamma_1 2\pi R_1 + \beta\gamma_2 2\pi R_2 + O(1) \quad (3.34)$$

The surface tension for each boundary is given by

$$\beta\gamma_i = -\frac{m}{4\pi} \left[\alpha_i \ln \frac{2N}{R_i} + 1 - \pi + \alpha_i + \frac{1 - \alpha_i^2}{\alpha_i} \ln(\alpha_i + 1) \right] \quad (3.35)$$

where $i = 1$ for the inner boundary and $i = 2$ for the outer boundary. The cutoff N should be chosen [11] as R/a where here $R = R_2 x^{-x^2/(1-x^2)}$ with $x = R_1/R_2$ in order to insure extensivity and recover for the bulk pressure p_b the same expression (3.26) as before.

In the limit $a \rightarrow 0$ the leading term of the surface tension is the same as in the slab and disk geometry

$$\beta\gamma \sim -\frac{\alpha m}{4\pi} \ln \frac{2}{ma} \quad (3.36)$$

for a wall with adhesivity α .

In equation (3.34) we do not find any logarithmic finite-size correction. There are some terms of the form $\ln R_2/R_1$ which are order 1 because R_2/R_1 is finite. This is in accordance with the expected formula (3.24) for an annulus where the Euler characteristic is $\chi = 0$. Here again the special attractive nature of the walls does not modify the universal finite-size correction.

As a conclusion to this part we might say that the logarithmic correction is really universal, not only it does not depend on the microscopic constitution of the system but also it is insensitive to the existence of a short-range one-body potential near the walls.

C. The disjoining pressure

Let us first detail the case of the disk geometry. The pressure p is given in terms of the grand potential Ω by

$$p = -\frac{1}{2\pi R} \frac{\partial \Omega}{\partial R} \quad (3.37)$$

Using equation (3.17) together with equations (3.18) and (3.19) gives

$$p = p_{\text{hd}} + p_{\text{at}} \quad (3.38)$$

where p_{hd} is the pressure for a disk with hard walls boundaries given by

$$\beta p_{\text{hd}} = \frac{m}{\pi R} \sum_{l=0}^{\infty} \frac{I_{l+1}(mR)}{I_l(mR)} \quad (3.39)$$

and p_{at} is the contribution to the pressure due to the attractive potential near the walls and it is given by

$$\beta p_{\text{at}} = \frac{\alpha}{2\pi R^2} \sum_{l=0}^{\infty} \frac{mR [I_l^2(mR) - I_{l+1}^2(mR)] - (2l+1)I_{l+1}(mR)I_l(mR)}{I_l(mR) [I_l(mR) + \alpha I_{l+1}(mR)]} \quad (3.40)$$

To study the stability of the system against an external applied pressure one should study the disjoining pressure

$p_d = p - p_b$ defined as the difference between the pres-

sure of the system and the pressure of an infinite system (the bulk pressure). Let us first consider the case $\alpha = 0$. A proper way to subtract the bulk pressure from expression (3.39) is by using the equation of state of the infinite system [9]

$$\beta p_b = \frac{1}{2}n_b + \frac{m^2}{4\pi} \quad (3.41)$$

where n_b is the bulk total density. A simple scaling argument shows that for $\beta q^2 < 2$ the equation of state of the two-dimensional two-component plasma is [20]

$$\beta p_b = [1 - (\beta q^2/4)]n_b \quad (3.42)$$

For $\beta q^2 = 2$, the case considered here, the introduction of a cutoff a is needed in order to avoid divergences but this breaks the scale invariance of the two-dimensional logarithmic Coulomb potential giving rise to the anomalous term ($m^2/4\pi$) in the equation of state. Notice that when the cutoff $a \rightarrow 0$ both p_b and n_b diverge and we have $\beta p_d/n_b = 1/2$ in accordance to the general equation of state (3.42).

Formally, the bulk density can be written as (see next section for details)

$$\begin{aligned} n_b &= \frac{m^2}{\pi} \sum_{l=-\infty}^{+\infty} I_l(mR)K_l(mR) \\ &= \frac{m^2}{\pi} \left[I_0 K_0 + 2 \sum_{l=1}^{\infty} I_l K_l \right] \end{aligned} \quad (3.43)$$

In the above expression and below the omitted argument of the Bessel functions is mR unless stated otherwise. On the other hand using the Wronskian [21] $I_l K_{l+1} + I_{l+1} K_l = (1/mR)$ the hard disk pressure (3.39) can be formally written as

$$\beta p_{\text{hd}} = \frac{m^2}{\pi} \left[\sum_{l=0}^{\infty} \frac{I_{l+1}^2 K_l}{I_l} + \sum_{l=1}^{\infty} I_l K_l \right] \quad (3.44)$$

Then the disjoining pressure for $\alpha = 0$ is given by

$$\beta(p_{\text{hd}} - p_b) = \beta p_{\text{hd,disj}} = \frac{m^2}{\pi} \left[\sum_{l=0}^{\infty} \frac{I_{l+1}^2 K_l}{I_l} - \frac{I_0 K_0}{2} - \frac{1}{4} \right] \quad (3.45)$$

Although the pressure p_{hd} and the bulk pressure p_b are divergent when the cutoff a vanishes, the disjoining pressure $p_{\text{hd,disj}}$ in the case $\alpha = 0$ proves to be well-defined for $a \rightarrow 0$ and the series (3.45) is convergent.

A plot of the disjoining pressure $p_{\text{hd,disj}}$ for a hard wall disk as a function of the radius R is shown in Figure 1. Notice that $p_{\text{hd,disj}}$ is an increasing function of R and it is always negative. This shows that in the absence of the attractive potential on the walls the system is always unstable for any radius R . This is a common feature of the disk geometry with the slab geometry studied in our previous work [3]. The system without any attractive potential on the boundary ($\alpha = 0$) is naturally unstable.

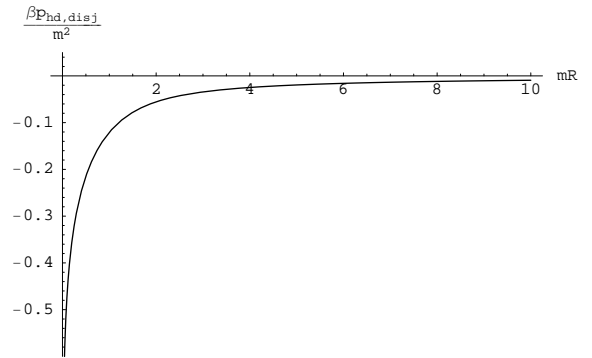


FIG. 1: The disjoining pressure $p_{\text{hd,disj}}$ for the disk in the case of non-attractive boundaries ($\alpha = 0$) as a function of the radius R . Notice that the disjoining pressure is always negative and it is an increasing function of the radius, indicating that the system is always unstable.

For $\alpha \neq 0$, the disjoining pressure p_d is given by

$$p_d = p_{\text{hd,disj}} + p_{\text{atd}} \quad (3.46)$$

with p_{atd} given by equation (3.40). Before proceeding one should be aware of an important fact. Although the first term $p_{\text{hd,disj}}$ is finite when the cutoff $a \rightarrow 0$ the second term on the other hand is divergent when $a \rightarrow 0$. The sum in equation (3.40) should be cutoff to an upper limit $N = R/a$ as it was done in the preceding section. Rigorously speaking when $a \rightarrow 0$ the dominant term for the disjoining pressure is p_{atd} . For large radius R , from last section results (3.30) and (3.36) on the finite-size corrections we can deduce the dominant term of the disjoining pressure when $a \rightarrow 0$

$$\begin{aligned} \beta p_d &\sim -\frac{1}{R} \beta \gamma \\ &\sim \frac{\alpha m}{4\pi R} \ln \frac{2}{ma} \end{aligned} \quad (3.47)$$

This term is always positive and is a decreasing function of R indicating that the system is always stable.

This is an important difference between the slab geometry studied in Ref. [3] and the present case of the disk. In the slab geometry the disjoining pressure is always finite for $a = 0$ and any value of α . For a slab of width W , the large- W expansion of the grand potential per unit area ω reads [3]

$$\omega = -p_b W + 2\gamma + O(e^{-mW}) \quad (3.48)$$

Then the pressure $p = \partial\omega/\partial W$ does not contain any contribution from the surface tension. On the other hand in the disk geometry considered here the existence of the curvature makes the surface tension γ very relevant for the disjoining pressure (see equation (3.47)) and since γ diverges logarithmically with the cutoff it plays a dominant role in the stability of the system.

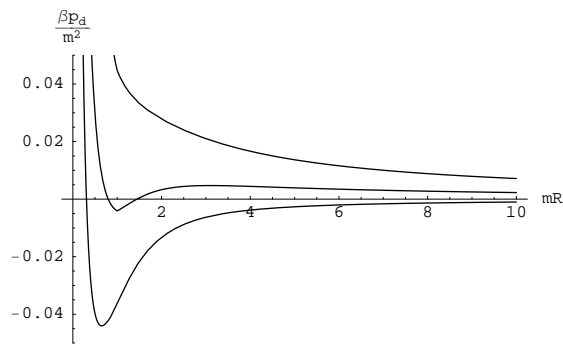


FIG. 2: The disjoining pressure p_d for the disk as a function of the radius R for $\alpha = 0.15, 0.21$ and 0.3 from bottom to top. The cutoff is chosen as $ma = 10^{-3}$. The case $\alpha = 0.3$ shows a stable disk for all radius, in the case $\alpha = 0.15$ only small disks are stable and when $\alpha = 0.21$ there is the possibility of a collapse from large disks to small disks.

Let us now consider a small but non-zero cutoff a . It is expected that the results of our theory in that case should be close to the ones of a model of small hard-core particles of diameter a . Then there will be a competition between the natural unstable behavior of the case without attractive potential ($\alpha = 0$) and the attractive part to the pressure p_{atd} which is stabilizing.

Figure 2 shows several plots of the disjoining pressure p_d as a function of the radius R for three special values of the adhesivity $\alpha = 0.15, 0.21$ and 0.3 for a fixed cutoff $ma = 10^{-3}$. These three plots show three characteristic regimes in which the system can be.

For large values of the adhesivity, for example the case $\alpha = 0.3$ shown in the Figure 2, the disjoining pressure is always positive and a decreasing function of the radius R . This is a normal behavior: if the system is compressed the internal pressure increases. This indicates a stable system for all values of the radius R .

In the case $\alpha = 0.15$ (small values of the adhesivity) we have two different behaviors of the disjoining pressure. For radius R smaller than a certain “critical” radius R_c , the disjoining pressure is a decreasing function of the radius R , indicating again a stable system. However, for radius R larger than R_c the disjoining pressure is an increasing function of the radius R . This behavior is anomalous, indicating that in this range of radius the system is not stable. A very large disk $R \rightarrow \infty$ is marginally stable and will collapse to a disk of smaller radius R^* where R^* is the radius corresponding to $p_d = 0$ (see Figure 3).

For $\alpha = 0.21$ (intermediate values of the adhesivity) we have a crossover regime. There are now three different behaviors of the pressure characterized by two special radius $R_c^{(1)}$ and $R_c^{(2)}$. For $R < R_c^{(1)}$ the pressure is a decreasing function of R : a stable regime. Then for $R_c^{(1)} < R < R_c^{(2)}$ the pressure is an increasing function of R : an unstable regime. Finally for $R > R_c^{(2)}$ the pres-

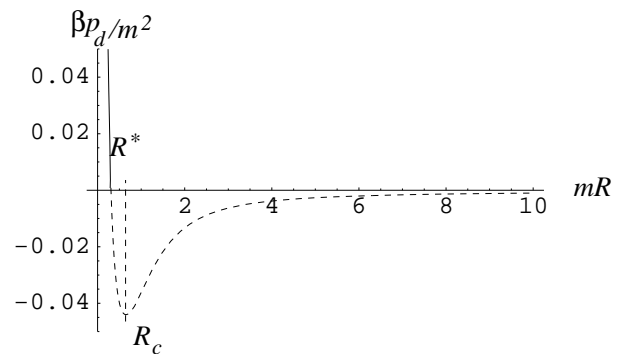


FIG. 3: The disjoining pressure p_d for the disk as a function of the radius R for $\alpha = 0.15$. The cutoff is chosen as $ma = 10^{-3}$. The radius R_c is defined by $\frac{\partial p_d}{\partial R} = 0$. A very large disk $R \rightarrow \infty$ would collapse to a disk of radius R^* with disjoining pressure $p_d(R^*) = 0$. The dashed region for $R > R^*$ is not physical.

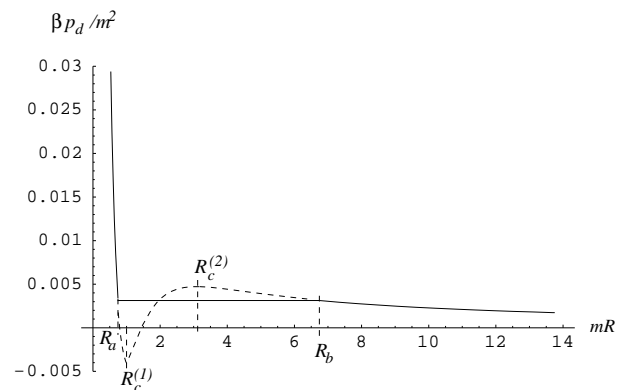


FIG. 4: The disjoining pressure p_d as a function of the radius R for $\alpha = 0.21$ and a cutoff $ma = 10^{-3}$. The theoretical result for the pressure shows a non-physical region (dashed line). The correct p_d vs. R curve can be obtained by a Maxwell construction, thus showing that in this case there is a first order transition (collapse) from a large (but finite) disk (radius R_b) to smaller disk with radius R_a (see Figure 4).

sure is again a decreasing function of R : another stable regime. One can do a Maxwell construction to determine the correct dependency of the pressure against the radius as shown in Figure 4. In this regime there is a first order transition (collapse) from a large (but finite) disk (radius R_b) to smaller disk with radius R_a (see Figure 4).

Two of the three regimes illustrated here, small adhesivity (for example $\alpha = 0.15$) and large adhesivity (for example $\alpha = 0.3$), also occur for the slab geometry studied in Ref. [3]. In that case they were separated by the special value $\alpha = \alpha_c = 1$. The disk case considered here is however more rich since there is also a crossover regime between the two, for intermediate values of α (for example $\alpha = 0.21$), with the possibility of stable large radius R disks, a forbidden (unstable) intermediate range of radius R and then again stable small disks.

The values of α characterizing the different regimes are however highly dependent on the cutoff and so are

the values of the ‘‘critical’’ radius R_c , $R_c^{(1)}$ and $R_c^{(2)}$. The values $\alpha = 0.15, 0.21$ and 0.3 of Figure 2 are for a cutoff $ma = 10^{-3}$, for other values of the cutoff these values will change. For this reason the analysis above should be considered with some care. For very small values of the cutoff a we expect that the results obtained here should reproduce asymptotically those of a primitive model of hard-core particles with radius a .

To conclude this section let us mention that in the annulus geometry the situation will be similar to the disk one. In that case one can consider the pressure on the inner boundary or the pressure on the outer boundary. For both pressures the dominant term when the cutoff $a \rightarrow 0$ will be given in terms of the surface tension γ as in equation (3.47). Then in the strict limit $a \rightarrow 0$ the annulus geometry will be stable if $\alpha > 0$ as in the disk case. Considering a small but non-zero cutoff a will lead to a similar discussion as in the disk with different regimes some of them exhibiting a collapse.

IV. THE DENSITY PROFILES

In this section, we study the densities of the Coulomb system confined inside a disk and inside an annulus. The densities can be obtained by computing the Green functions introduced in Sec. II. First we will solve and extensively study model I for the disk then the annulus. Then we will briefly consider the results that can be obtained using model II.

A. The disk

In the disk geometry, for model I, the fugacity $m_-(\mathbf{r})$ is given by Eq. (2.10). From Eq. (2.9), when $r_2 \neq R$, we see that G_{--} and G_{-+} are continuous for $r_1 = R$. However because of the Dirac delta distribution in the definition of $m_-(r)$ the functions G_{+-} and G_{++} are discontinuous at $r_1 = R$. The discontinuity can be obtained from Eq. (2.9) if $r_2 \neq r_1$:

$$\begin{aligned} G_{+\mp}(r_1 = R^-, r_2) - G_{+\mp}(r_1 = R^+, r_2) \\ = \alpha e^{-i\theta_1} G_{-\mp}(r_1 = R, r_2) \end{aligned} \quad (4.1)$$

If both points \mathbf{r}_1 and \mathbf{r}_2 are inside the disk but not on the boundary then Eq. (2.9) lead to a Helmholtz equation for G_{++} and for G_{--}

$$[m^2 - \Delta] G_{\pm\pm}(\mathbf{r}_1, \mathbf{r}_2) = m\delta(\mathbf{r}_1 - \mathbf{r}_2) \quad (4.2)$$

and the other Green functions can be obtained from

$$\frac{e^{\pm i\theta_1}}{m} \left(-\partial_{r_1} \mp \frac{i}{r_1} \partial_{\theta_1} \right) G_{\pm\pm}(\mathbf{r}_1, \mathbf{r}_2) = G_{\mp\pm}(\mathbf{r}_1, \mathbf{r}_2) \quad (4.3)$$

Equation (4.2) has solutions of the form

$$\begin{aligned} G_{\pm\pm}(\mathbf{r}_1, \mathbf{r}_2) = \frac{m}{2\pi} \sum_{l=-\infty}^{+\infty} e^{il(\theta_1 - \theta_2)} [I_l(mr_<)K_l(mr_>) \\ + A_l^\pm(r_2)I_l(mr_1)] \end{aligned} \quad (4.4)$$

where $r_< = \min(r_1, r_2)$ and $r_> = \max(r_1, r_2)$. The remaining Green functions can be found using Eq. (4.3).

If \mathbf{r}_1 is outside the film while \mathbf{r}_2 is fixed inside the film $m_+(r_1) = m_-(r_1) = 0$, the $G_{s_1 s_2}$ that satisfy Eq. (2.9) are

$$G_{+\mp}(\mathbf{r}_1, \mathbf{r}_2) = \sum_{l=-\infty}^{+\infty} C_l(r_2, \theta_2) (r_1 e^{i\theta_1})^l, \quad (4.5)$$

$$G_{-\mp}(\mathbf{r}_1, \mathbf{r}_2) = \sum_{l=-\infty}^{+\infty} D_l(r_2, \theta_2) (r_1 e^{-i\theta_1})^{-l}. \quad (4.6)$$

So, in order to have finite solutions at $r_1 = \infty$ it is necessary that for $r_1 > R$

$$\begin{aligned} C_l(r_2, \theta_2) = 0 \quad \text{for } l \geq 0 \\ D_l(r_2, \theta_2) = 0 \quad \text{for } l \leq 0, \end{aligned} \quad (4.7)$$

Eqs. (4.1) and (4.7) are the boundary conditions that complement the differential equations (4.2) and (4.3) for the Green functions.

Solving for the coefficients A_l^\pm , we arrive at the following expressions for the Green functions for $0 \leq r_{1,2} < R$:

$$\begin{aligned} G_{++}(\mathbf{r}_1, \mathbf{r}_2) = \frac{m}{2\pi} K_0(m|\mathbf{r}_1 - \mathbf{r}_2|) \\ + \frac{m}{2\pi} \sum_{l=0}^{+\infty} e^{il(\theta_1 - \theta_2)} \left[\frac{K_l}{I_l} I_{l+1}(mr_1) I_{l+1}(mr_2) \right. \\ \left. + \frac{\alpha K_{l+1} - K_l}{\alpha I_{l+1} + I_l} I_l(mr_1) I_l(mr_2) \right] \end{aligned} \quad (4.8)$$

and

$$\begin{aligned} G_{--}(\mathbf{r}_1, \mathbf{r}_2) = \frac{m}{2\pi} K_0(m|\mathbf{r}_1 - \mathbf{r}_2|) \\ - \frac{m}{2\pi} \sum_{l=0}^{+\infty} e^{il(\theta_1 - \theta_2)} \left[\frac{K_l}{I_l} I_l(mr_1) I_l(mr_2) \right. \\ \left. + \frac{\alpha K_{l+1} - K_l}{\alpha I_{l+1} + I_l} I_{l+1}(mr_1) I_{l+1}(mr_2) \right] \end{aligned} \quad (4.9)$$

with I_l meaning $I_l(mR)$, and the same convention for the Bessel function K_l .

The one-particle densities are given in terms of these Green functions as

$$\rho_s(\mathbf{r}) = m_s(r) G_{ss}(\mathbf{r}, \mathbf{r}) \quad (4.10)$$

As we explained in section II the continuous limit model presents divergences in the expressions of the densities.

This is seen in the term $K_0(mr_{12})$ that diverges logarithmically as $r_{12} = |\mathbf{r}_1 - \mathbf{r}_2| \rightarrow 0$. So we impose a short distance cutoff a . One can think that particles are disks of diameter a , so the minimal distance between particles is a .

The first term in Eqs. (4.8) and (4.9) gives the bulk density ρ_b , the density of the unbounded system as calculated in Ref. [9]. For $a \rightarrow 0$

$$\rho_b^+ = \rho_b^- = \rho_b = \frac{m^2}{2\pi} K_0(ma) \sim \frac{m^2}{2\pi} \left[\ln \frac{2}{ma} - \gamma \right] \quad (4.11)$$

where $\gamma \simeq 0.5772$ is the Euler constant. In the second terms of Eqs. (4.8) and (4.9) the sum can eventually di-

verge when $\mathbf{r}_1 = \mathbf{r}_2 = \mathbf{r}$ for certain values of \mathbf{r} (in the boundaries) so we should impose a cutoff $|l| < N = R/a$ as it has been done in the expressions of the pressure and grand-potential obtained in the last section.

Because of the form (2.10) of $m_-(r)$, the negative density can be written as

$$\rho_-(r) = \left(1 + \frac{\alpha}{m} \delta(r - R) \right) \rho_-^*(r) \quad (4.12)$$

where ρ_-^* can be seen as the density of non-adsorbed particles. For the positive particles $\rho_+ = \rho_+^*$. Finally we have

$$\rho_+^*(r) = \rho_b + \frac{m^2}{2\pi} \sum_{l=0}^{\infty} \left[\frac{K_l}{I_l} I_{l+1}^2(mr) + \frac{\alpha K_{l+1} - K_l}{\alpha I_{l+1} + I_l} I_l^2(mr) \right] \quad (4.13a)$$

$$\rho_-^*(r) = \rho_b - \frac{m^2}{2\pi} \sum_{l=0}^{\infty} \left[\frac{K_l}{I_l} I_l^2(mr) + \frac{\alpha K_{l+1} - K_l}{\alpha I_{l+1} + I_l} I_{l+1}^2(mr) \right] \quad (4.13b)$$

The non-adsorbed charge density $\rho^* = \rho_+^* - \rho_-^*$ can be obtained from the above expression and using the Wronskian of the Bessel functions $I_l K_{l+1} + I_{l+1} K_l = 1/mR$,

$$\rho^*(r) = \frac{\alpha m^2}{2\pi R} \sum_{l=0}^{\infty} \frac{I_{l+1}^2(mr) + I_l^2(mr)}{(\alpha I_{l+1} + I_l) I_l} \quad (4.14)$$

Finally, the total charge density

$$\begin{aligned} \rho(r) &= \rho_+(r) - \rho_-(r) \\ &= \rho_+(r) - \left(1 + \frac{\alpha}{m} \delta(r - R) \right) \rho_-^*(r) \\ &= \rho^*(r) - \sigma_- \delta(r - R) \end{aligned} \quad (4.15)$$

has a non-adsorbed part $\rho^*(r)$ and a adsorbed ‘‘surface’’ charge density in the boundary

$$\sigma_- = \frac{\alpha}{m} \rho_-^*(R) \quad (4.16)$$

This surface charge density σ_- comes from the $\delta(r - R)$ part of the negative charge density. Writing formally the bulk part of the density as $\rho_b = (m^2/2\pi) \sum_{l \in \mathbb{Z}} I_l K_l$ one can obtain the following expression for σ_- from Eqs. (4.16) and (4.13b)

$$\sigma_- = \frac{\alpha}{2\pi R} \sum_{l=0}^{\infty} \frac{I_{l+1}}{\alpha I_{l+1} + I_l} \quad (4.17)$$

Actually the adsorbed charge density should obey two special relations. The first is a sum rule that expresses the global electro-neutrality of the system

$$R \sigma_- = \int_0^R \rho^*(r) r dr \quad (4.18)$$

Using the indefinite integral

$$\int^{mR} x (I_{l+1}^2(x) + I_l^2(x)) dx = \frac{(mR)^2}{2} [I_{l+1}^2 - I_l I_{l+2} + I_l^2 - I_{l-1} I_{l+1}] = mR I_l I_{l+1} \quad (4.19)$$

obtained using the recurrence relations [21] for the Bessel functions I_l , the sum rule (4.18) is immediately shown to be satisfied.

On the other hand the adhesivity α can be thought as

a sort of fugacity that controls the number of adsorbed particles [1] and one can obtain the total number of adsorbed particles $2\pi R \sigma_-$ from the grand potential Ω by

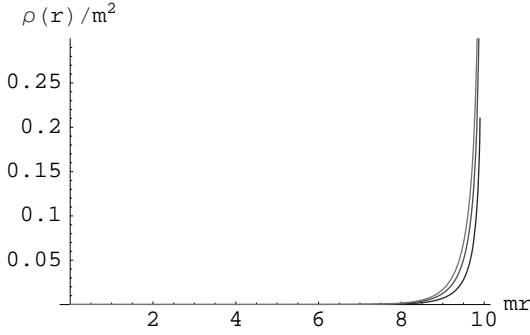


FIG. 5: The charge density profile $\rho(r)$ for a disk of radius $R = 10/m$. From bottom to top the adhesivity $\alpha = 0.25, 0.5, 0.75$.

using the usual thermodynamic relation

$$2\pi R \sigma_- = -\alpha \beta \frac{\partial \Omega}{\partial \alpha} \quad (4.20)$$

This relationship is also immediately shown to be satisfied from the expression (3.19) for $\Omega_{\text{at}}^{\text{D}}$, the part of the grand potential that depends on α .

For a large disk, $R \rightarrow \infty$, the dominant part of the grand potential that depends on α is the surface tension γ given by equations (3.31) and (3.36). Then we have

$$\sigma_- = -\beta \alpha \frac{\partial \gamma}{\partial \alpha} \quad (4.21)$$

a relation already shown to be true in Ref. [3] for the same system near a plane attractive hard wall. Using Eq. (3.31) into Eq. (4.21) gives explicitly

$$\sigma_- = \frac{m}{4\pi} \left[\alpha \ln \frac{2}{ma} - \frac{\alpha^2 + 1}{\alpha} \ln(\alpha + 1) + 1 \right] \quad (4.22)$$

Thus recovering a known result from Ref. [3]. Notice that for large disks the adsorbed surface charge density becomes independent of the radius R . This result can of course be also obtained directly from Eq. (4.17) in the limit of large- R using the Debye expansions (3.28) of the Bessel functions.

In Figure 5, we can see the charge density profile $\rho(r)$ (actually only the non-adsorbed part $\rho^*(r)$ is shown). It can be seen that the negative surface charge $-\sigma_-$ (not shown in the figure) is screened by a positive layer near $r = R$. As the adhesivity is increased, σ_- increases, and therefore the density of the screening positive layer shown in Figure 5 increases. This screening layer has a thickness of order of magnitude m^{-1} as expected since m^{-1} is a measure of the screening length [9].

In Figure 6, we can see the distribution of the negative particles (two lower curves) and positive particles (two upper curves). The negative particles feel repelled by

the ones that lie in the boundary (the surface charge σ_-). Therefore, the negative density $\rho_-(r)$ decreases near the

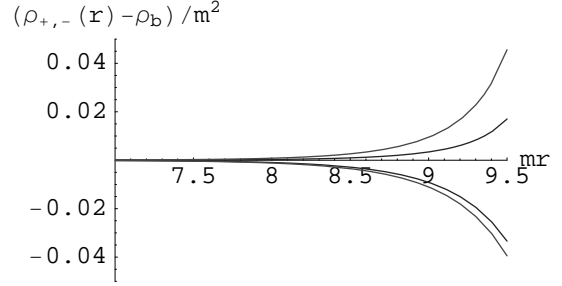


FIG. 6: The density profiles $\rho_+(r)$ and $\rho_-(r)$ for a disk of radius $R = 10/m$. The bulk density has been subtracted from both densities. The upper curves correspond to the density of the positive particles $\rho_+(r)$ and the bottom curves to the density of the negative particles $\rho_-(r)$. The adhesivity $\alpha = 1$ for the topmost curve ($\rho_+(r)$) and the bottommost curve ($\rho_-(r)$). The two other curves correspond to $\alpha = 0.5$.

frontier. The positive charge density $\rho_+(r)$ inside the disk can be observed in the upper curves of Figure 6. Due to the large accumulation of negative charges at the frontier, the positive particles tend to shield this charge. Hence, there is an increase of the positive density near R .

As we increase the adhesivity, the negative adsorbed charge on the border gets larger while on the inner region there is a stronger repulsion of the negative charges and an increase in the number of positive particles shielding the outer charge.

B. The Annulus

For the annulus geometry with a delta distribution modeling the external attractive potential (model I), we follow the same reasonings as for the disk geometry. The solution to Eq. (4.2) for $R_1 < r < R_2$ is of the form

$$G_{\pm\pm}(\mathbf{r}_1, \mathbf{r}_2) = \frac{m}{2\pi} \sum_{l=-\infty}^{+\infty} e^{il\theta_{12}} [I_l(mr_{<})K_l(mr_{>}) + A_l^{\pm}(r_2)I_l(mr_1) + B_l^{\pm}(r_2)K_l(mr_1)] \quad (4.23)$$

where we defined $\theta_{12} = \theta_1 - \theta_2$. As in the disk case, the Green functions G_{--} and G_{-+} are continuous while G_{++} and G_{+-} are discontinuous at $r = R_1$ and $r = R_2$ with a discontinuity given by Eq. (4.1) replacing the adhesivity α by α_1 for the discontinuity at $r = R_1$ and by α_2 for the discontinuity at $r = R_2$.

Solving for the coefficients we finally find

$$G_{--}(\mathbf{r}_1, \mathbf{r}_2) = \frac{m}{2\pi} K_0(m|\mathbf{r}_1 - \mathbf{r}_2|) \quad (4.24a)$$

$$- \frac{m}{2\pi} \sum_{l=0}^{\infty} \frac{e^{-il\theta_{12}} A_l^{(1)}}{D_l^{(1)}} I_l(mr_1) I_l(mr_2) \quad (4.24b)$$

$$- \frac{m}{2\pi} \sum_{l=0}^{\infty} \frac{e^{-il\theta_{12}} B_l^{(1)}}{D_l^{(1)}} K_l(mr_1) K_l(mr_2) \quad (4.24c)$$

$$+ \frac{m}{2\pi} \sum_{l=0}^{\infty} \frac{e^{-il\theta_{12}} C_l^{(1)}}{D_l^{(1)}} [I_l(mr_1) K_l(mr_2) + K_l(mr_1) I_l(mr_2)] \quad (4.24d)$$

$$+ \frac{m}{2\pi} \sum_{l=0}^{\infty} \frac{e^{i(l+1)\theta_{12}} A_l^{(2)}}{D_l^{(2)}} I_{l+1}(mr_1) I_{l+1}(mr_2) \quad (4.24e)$$

$$+ \frac{m}{2\pi} \sum_{l=0}^{\infty} \frac{e^{i(l+1)\theta_{12}} B_l^{(2)}}{D_l^{(2)}} K_{l+1}(mr_1) K_{l+1}(mr_2) \quad (4.24f)$$

$$- \frac{m}{2\pi} \sum_{l=0}^{\infty} \frac{e^{i(l+1)\theta_{12}} C_l^{(2)}}{D_l^{(2)}} [K_{l+1}(mr_1) I_{l+1}(mr_2) + I_{l+1}(mr_1) K_{l+1}(mr_2)] \quad (4.24g)$$

and

$$G_{++}(\mathbf{r}_1, \mathbf{r}_2) = \frac{m}{2\pi} K_0(m|\mathbf{r}_1 - \mathbf{r}_2|) \quad (4.25a)$$

$$+ \frac{m}{2\pi} \sum_{l=0}^{\infty} \frac{e^{-i(l+1)\theta_{12}} A_l^{(1)}}{D_l^{(1)}} I_{l+1}(mr_1) I_{l+1}(mr_2) \quad (4.25b)$$

$$+ \frac{m}{2\pi} \sum_{l=0}^{\infty} \frac{e^{-i(l+1)\theta_{12}} B_l^{(1)}}{D_l^{(1)}} K_{l+1}(mr_1) K_{l+1}(mr_2) \quad (4.25c)$$

$$+ \frac{m}{2\pi} \sum_{l=0}^{\infty} \frac{e^{-i(l+1)\theta_{12}} C_l^{(1)}}{D_l^{(1)}} [I_{l+1}(mr_1) K_{l+1}(mr_2) + K_{l+1}(mr_1) I_{l+1}(mr_2)] \quad (4.25d)$$

$$- \frac{m}{2\pi} \sum_{l=0}^{\infty} \frac{e^{il\theta_{12}} A_l^{(2)}}{D_l^{(2)}} I_l(mr_1) I_l(mr_2) \quad (4.25e)$$

$$- \frac{m}{2\pi} \sum_{l=0}^{\infty} \frac{e^{il\theta_{12}} B_l^{(2)}}{D_l^{(2)}} K_l(mr_1) K_l(mr_2) \quad (4.25f)$$

$$- \frac{m}{2\pi} \sum_{l=0}^{\infty} \frac{e^{il\theta_{12}} C_l^{(2)}}{D_l^{(2)}} [I_l(mr_1) K_l(mr_2) + K_l(mr_1) I_l(mr_2)] \quad (4.25g)$$

with

$$A_l^{(1)} = K_l^{(2)} \left(\alpha_1 K_l^{(1)} + K_{l+1}^{(1)} \right) \quad (4.26a)$$

$$B_l^{(1)} = I_l^{(2)} \left(\alpha_1 I_l^{(1)} - I_{l+1}^{(1)} \right) \quad (4.26b)$$

$$C_l^{(1)} = K_l^{(2)} \left(\alpha_1 I_l^{(1)} - I_{l+1}^{(1)} \right) \quad (4.26c)$$

$$D_l^{(1)} = I_l^{(2)} \left(\alpha_1 K_l^{(1)} + K_{l+1}^{(1)} \right) - K_l^{(2)} \left(\alpha_1 I_l^{(1)} - I_{l+1}^{(1)} \right) \quad (4.26d)$$

$$A_l^{(2)} = K_{l+1}^{(1)} \left(\alpha_2 K_{l+1}^{(2)} - K_l^{(2)} \right) \quad (4.26e)$$

$$B_l^{(2)} = I_{l+1}^{(1)} \left(\alpha_2 I_{l+1}^{(2)} + I_l^{(2)} \right) \quad (4.26f)$$

$$C_l^{(2)} = I_{l+1}^{(1)} \left(\alpha_2 K_{l+1}^{(2)} - K_l^{(2)} \right) \quad (4.26g)$$

$$D_l^{(2)} = I_{l+1}^{(1)} \left(\alpha_2 K_{l+1}^{(2)} - K_l^{(2)} \right) - K_{l+1}^{(1)} \left(\alpha_2 I_{l+1}^{(2)} + I_l^{(2)} \right) \quad (4.26h)$$

where $I_l^{(1)} = I_l(mR_1)$, $I_l^{(2)} = I_l(mR_2)$ and the same convention for the other Bessel functions.

The individual densities are obtained putting $\mathbf{r}_1 = \mathbf{r}_2 = \mathbf{r}$ in the above expressions since $\rho_s(r) = m_s(\mathbf{r})G_{ss}(\mathbf{r}, \mathbf{r})$. The above expressions are quite long, however one can notice some symmetries between G_{--} and G_{++} . Beside a change of sign and the phase factor (which is irrelevant in the calculation of the densities) the coefficient of the term $I_l(mr_1)I_l(mr_2)$ in G_{--} is the same as the one for $I_{l+1}(mr_1)I_{l+1}(mr_2)$ in G_{++} and so

on. The charge density can be written again as

$$\rho(r) = \rho^*(r) - \sigma_-^{(1)}\delta(r - R_1) - \sigma_-^{(2)}\delta(r - R_2) \quad (4.27)$$

with a non-absorbed part $\rho^*(r)$ and a surface density

$$\sigma_-^{(1,2)} = (\alpha_{1,2}/m)\rho_-^*(R_{1,2}) \quad (4.28)$$

of adsorbed negative particles in R_1 and R_2 respectively. The non-adsorbed charge density is

$$\begin{aligned} \rho^*(r) = \frac{m^2}{2\pi} \sum_{l=0}^{\infty} \left[(C_{1,l}^{II} + C_{2,l}^{II}) [I_{l+1}^2(mr) + I_l^2(mr)] + (C_{1,l}^{KK} + C_{2,l}^{KK}) [K_{l+1}^2(mr) + K_l^2(mr)] \right. \\ \left. + 2(C_{1,l}^{IK} + C_{2,l}^{IK}) [I_{l+1}(mr)K_{l+1}(mr) - I_l(mr)K_l(mr)] \right] \end{aligned} \quad (4.29)$$

with the coefficients that depend on α_1 given by

$$C_{1,l}^{II} = \frac{A_l^{(1)}}{D_l^{(1)}}, \quad C_{1,l}^{KK} = \frac{B_l^{(1)}}{D_l^{(1)}}, \quad C_{1,l}^{IK} = \frac{C_l^{(1)}}{D_l^{(1)}} \quad (4.30)$$

and the ones that depend on α_2 are

$$C_{2,l}^{II} = -\frac{A_l^{(2)}}{D_l^{(2)}}, \quad C_{2,l}^{KK} = -\frac{B_l^{(2)}}{D_l^{(2)}}, \quad C_{2,l}^{IK} = \frac{C_l^{(2)}}{D_l^{(2)}} \quad (4.31a)$$

The adsorbed charge density in each boundary can be computed by replacing $G_{--}(R_{1,2}, R_{1,2})$ from Eq. (4.24) into Eq. (4.28) or by using the thermodynamic relation

$$2\pi R_{1,2} \sigma_-^{(1,2)} = -\alpha_{1,2} \beta \frac{\partial \Omega^A}{\partial \alpha_{1,2}} \quad (4.32)$$

Either way the result is the same as expected

$$\sigma_-^{(1)} = \frac{\alpha_1}{2\pi R_1} \sum_{l=0}^{\infty} \frac{I_l^{(2)} K_l^{(1)} - K_l^{(2)} I_l^{(1)}}{D_l^{(1)}} \quad (4.33a)$$

$$\sigma_-^{(2)} = \frac{\alpha_2}{2\pi R_2} \sum_{l=0}^{\infty} \frac{I_{l+1}^{(2)} K_{l+1}^{(1)} - K_{l+1}^{(2)} I_{l+1}^{(1)}}{D_l^{(2)}} \quad (4.33b)$$

Using the indefinite integrals (4.19) and [22]

$$\int^{mR} (K_l^2(x) + K_{l+1}^2(x)) x dx = -mR K_{l+1} K_l \quad (4.34)$$

$$\int^{mR} (I_{l+1}(x)K_{l+1}(x) - I_l(x)K_l(x)) x dx = \frac{mR}{2}(K_{l+1}I_l - I_{l+1}K_l) \quad (4.35)$$

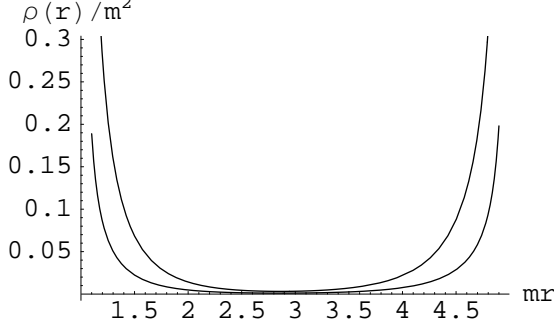


FIG. 7: The charge density profile $\rho(r)$ for an disk of inner radius $R_1 = 1/m$ and outer radius $R_2 = 5/m$. The adhesivities in each boundary have been chosen equals $\alpha_1 = \alpha_2 = \alpha$. The upper curve correspond to $\alpha = 1$ while the lower one to $\alpha = 0.25$.

one can verify that the electroneutrality sum rule

$$\int_{R_1}^{R_2} \rho^*(r) r dr = R_1 \sigma_-^{(1)} + R_2 \sigma_-^{(2)} \quad (4.36)$$

is satisfied. For the reader interested in the details of this calculation, an extended version of this manuscript is available online [23].

Figure 7 shows a plot of the charge density $\rho(r)$ for an annulus with inner radius $R_1 = 1/m$ and outer radius $R_2 = 5/m$ for $\alpha_1 = \alpha_2 = 0.5$ and $\alpha_1 = \alpha_2 = 1$. In both figures one can see a positive layer of charge in each boundary screening the adsorbed negative surface charge densities $\sigma_-^{(1,2)}$. As $\alpha_{1,2}$ increases the adsorbed charge increases and so does the positive layer. Although it is not perfectly clear in Figure 7 there is actually slightly more adsorbed surface charge density in the inner boundary than in the outer. This can be seen in Figure 8 that shows the difference between the adsorbed surface charge in the inner boundary and the surface charge in the outer one, $\sigma_-^{(1)} - \sigma_-^{(2)}$, as a function of α . Figure 8 clearly shows that $\sigma_-^{(1)} > \sigma_-^{(2)}$ if $\alpha_1 = \alpha_2$. On the other hand the total charge on the inner boundary is smaller than the total charge on the outer boundary: $2\pi R_1 \sigma_-^{(1)} < 2\pi R_2 \sigma_-^{(2)}$. This can be seen directly from Eqs. (4.33). If $\alpha_1 = \alpha_2 = \alpha$, each term in the series of the difference $R_1 \sigma_-^{(1)} - R_2 \sigma_-^{(2)}$ from Eqs. (4.33) is of the

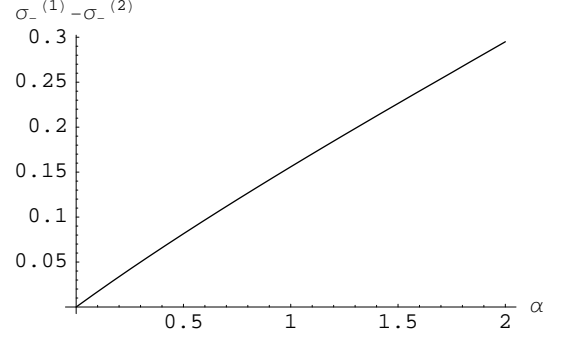


FIG. 8: The difference between the surface charge in the inner boundary and the surface charge in the outer one $\sigma_-^{(1)} - \sigma_-^{(2)}$ as a function of α for an annulus of inner radius $R_1 = 1/m$ and outer radius $R_2 = 5/m$.

form

$$\frac{\alpha}{D_l^{(1)} D_l^{(2)}} (b_l - b_{l+1}) \quad (4.37)$$

where $D_l^{(1)}$ and $D_l^{(2)}$ are the denominators in each term of the sums in Eqs. (4.33a) and (4.33b) respectively, and $b_l = K_l^{(1)} I_l^{(2)} - K_l^{(2)} I_l^{(1)}$. The sequence $(b_l)_{l \in \mathbb{N}}$ has the property of being monotonically increasing with l . Then we conclude $R_1 \sigma_-^{(1)} < R_2 \sigma_-^{(2)}$.

C. Model II

We now briefly consider model II and some of its results in the annulus geometry.

In the annulus geometry, there are two outer regions, each one has a width $\tilde{\delta}$, and an inner region that has a thickness $R_2 - R_1 - 2\tilde{\delta}$. We can distinguish three regions for the annulus geometry: the inner border $R_1 < r_1 < R_1 + \tilde{\delta}$ (region 1), the bulk of the film $R_1 + \tilde{\delta} < r_1 < R_2 - \tilde{\delta}$ (region 2) and the outer border $R_2 - \tilde{\delta} < r_1 < R_2$ (region 3). So for this model in the annulus geometry, we define the position dependent fugacities as

$$m_+(r_1) = m \quad (4.38a)$$

$$m_-(r_1) = \begin{cases} m_2 & \text{if } r_1 \in \text{region 1} \\ m & \text{if } r_1 \in \text{region 2} \\ m_2 & \text{if } r_1 \in \text{region 3} \end{cases} \quad (4.38b)$$

The fugacity in the border regions is $m_2 = m \exp(-\beta U_-)$ where $U_- < 0$ is the value of the external potential $V_-(\mathbf{r})$ near the boundary. Notice that $m_2 > m$. It is clear that model I is the limit of model II when $\tilde{\delta} \rightarrow 0$ and $m_2 \rightarrow \infty$ with the product $m_2 \tilde{\delta} = \alpha$ finite.

For this model II, the following symmetrization of the problem explained below will be useful. If an external potential is acting differently on positive and negative particles, as in our case, in order to symmetrize the problem for the two types of particles, Cornu and Jancovici [9] propose to define $m(\mathbf{r})$ and $V(\mathbf{r})$ by the relations

$$m_s(\mathbf{r}) = m(\mathbf{r}) \exp[-2sV(\mathbf{r})], \quad s = \pm 1 \quad (4.39)$$

where $V(\mathbf{r})$ in general is different from the external $V_{\pm}(\mathbf{r})$ potentials. Knowing that $V_-(\mathbf{r})$ is constant in each region, in terms of the modified Green functions

$$g_{s_1 s_2}(\mathbf{r}_1, \mathbf{r}_2) = e^{-s_1 V(\mathbf{r}_1)} G_{s_1 s_2}(\mathbf{r}_1, \mathbf{r}_2) e^{-s_2 V(\mathbf{r}_2)} \quad (4.40)$$

the system of equations (2.9) can be shown to be equivalent to

$$\left[(m(r_1))^2 - \Delta \right] g_{\pm\pm}(\mathbf{r}_1, \mathbf{r}_2) = m(r_1) \delta(\mathbf{r}_1 - \mathbf{r}_2) \quad (4.41)$$

$$\frac{e^{\pm i\theta_1}}{m(r_1)} \left(-\partial_{r_1} \mp \frac{i}{r_1} \partial_{\theta_1} \right) g_{\pm\pm}(\mathbf{r}_1, \mathbf{r}_2) = g_{\mp\pm}(\mathbf{r}_1, \mathbf{r}_2) \quad (4.42)$$

where Δ is the Laplacian operator and

$$m(r) = \begin{cases} m_0 = (mm_2)^{1/2} & \text{if } r \text{ in regions 1 or 3,} \\ m & \text{if } r \text{ in region 2.} \end{cases} \quad (4.43)$$

and the potential defined in Eq. (4.39) is given by

$$\exp(V(\mathbf{r})) = \begin{cases} (m_2/m)^{1/4} & \text{if } r \text{ in regions 1 or 3,} \\ 1 & \text{if } r \text{ in region 2.} \end{cases} \quad (4.44)$$

To obtain the Green functions $g_{\pm\pm}$ we solve Eq. (4.41) which is a standard inhomogeneous Helmholtz equation in each region: inner border $R_1 < r < R_1 + \tilde{\delta}$ (region 1), bulk $R_1 + \tilde{\delta} < r < R_2 - \tilde{\delta}$ (region 2) and outer border $R_2 - \tilde{\delta} < r < R_2$ (region 3). Outside the annulus $r < R_1$ and $r > R_2$ the fugacities vanish and the equation satisfied by $G_{\pm\pm}$ is the Laplace equation. The Green functions $G_{s_1 s_2}$ are continuous at each boundary $r = R_1$, $r = R_1 + \tilde{\delta}$, $r = R_2 - \tilde{\delta}$ and $r = R_2$. Remember that here the Green functions $G_{s_1 s_2}$ are different from the auxiliary functions $g_{s_1 s_2}$. Their relationship is given by Eq. (4.40). While the Green functions $G_{s_1 s_2}$ are continuous, the auxiliary Green functions $g_{s_1 s_2}$ are in general discontinuous at the interfaces.

In the regions of interest, the form of the solution is,

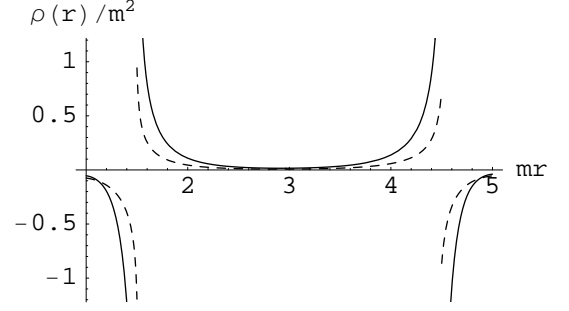


FIG. 9: The charge density profile for an annulus with inner radius $R_1 = 1/m$, outer radius $R_2 = 5/m$ in model II. The width of the borders are $\tilde{\delta} = 0.5/m$. The fugacity in the border regions is: for the solid line curve $m_2 = 16m$ corresponding to a value of $m_0 = 4m$ and for the dashed line curve $m_2 = 4m$ corresponding to a value of $m_0 = 2m$. The cutoff in the sums of Bessel functions in the expression of the density has been chosen as $N = 100$.

in general,

$$g_{\pm\pm}(\mathbf{r}_1, \mathbf{r}_2) = \frac{m(r_1)}{2\pi} \times \sum_{l=-\infty}^{+\infty} e^{il(\theta_1 - \theta_2)} [I_l(m(r_1)r_<)K_l(m(r_1)r_>) + B_l^{\pm}(r_2)I_l(m(r_1)r_1) + C_l^{\pm}(r_2)K_l(m(r_1)r_1)] \quad (4.45)$$

with $m(r) = m_0$ in the border regions 1 and 3 and $m(r) = m$ in the bulk region 2. Imposing the continuity of the Green functions $G_{s_1 s_2}$ gives a linear system of equations for the coefficients B_l^{\pm} and C_l^{\pm} which can be conveniently solved with the aid of matrix algebra software like MATHEMATICA.

The explicit expression of the coefficients obtained from the solution of the linear systems [15] are too long to reproduce here, however we show in Figure 9 a plot of charge density profile for two values of m_2 , $m_2 = 16m$ and $m_2 = 4m$.

The discontinuity of the charge density profile near the interfaces is due to the fact that the density profile of the negative particles is discontinuous there. This is expected for the negative particles since the potential $V_-(r)$ is discontinuous across the interfaces. It is clear from our formalism that the density profile should have the same kind of discontinuity that the Boltzmann factor of $V_-(r)$ since $\rho_-(r) = m_-(r) G_{--}(\mathbf{r}, \mathbf{r})$ with $m_-(r) = m \exp(-\beta V_-(r))$ and G_{--} continuous at the interfaces. Actually this is a more general result of statistical mechanics of inhomogeneous fluids at discontinuous interfaces. In general for a fluid with density $n(x)$ near a planar interface characterized by an external potential $V_{\text{ext}}(x)$ eventually discontinuous at $x = 0$ the y -function $\exp(\beta V_{\text{ext}}(x)) n(x)$ is continuous [24].

There is a higher density of particles (both negative and positive) in the borders than in the bulk: for higher

values of the fugacity m_2 in the border (the external potential $V_-(\mathbf{r})$ is more attractive), the density in the borders is higher. In region 2, the density far from the interfaces is close to the bulk value (4.11). In the borders, away from the interfaces the density tries to be close to the new bulk value given by Eq. (4.11) replacing m by m_0 . If the width $\tilde{\delta}$ of the border region was much larger than m_0^{-1} , one would expect that the density far away from the interfaces converges to a bulk value according to the value of $m(r)$ in that region. This is true for both the negative and positive of particles. Due to the natural tendency of the system to be electrically neutral, the positive particles try to follow the negative ones so the system is not locally charged. However at the interfaces $r = R_1 + \tilde{\delta}$ and $r = R_2 - \tilde{\delta}$ there remains a non-neutral charge density that can be seen in Figure 9. Actually one can see in Figure 9 a double charged layer. Inside the border region (1 or 3) there is a negative charge density layer and outside the border, in the bulk region 2, a positive layer, the same one that was previously observed with model I in Figure 7. These double layers are concentrated near the interfaces at $r = R_1 + \tilde{\delta}$ and at $r = R_2 - \tilde{\delta}$ and have a thickness of order m^{-1} for the positive layer in region 2 and m_0^{-1} for the negative layer in regions 1 and 3.

V. SUMMARY AND PERSPECTIVES

The present solvable model studied here gave us interesting information about the behavior of confined Coulomb systems with attractive boundaries. This system has an induced internal charge on the boundary which is created by an external potential which is not of electrical nature. This potential only acts on the negative particles, while the positive particles are unaffected. This is not the usual situation that has been studied extensively in the past, where the system is submitted to

electrical forces due to possible external charges.

First, we found that large systems exhibit the same finite-size corrections that for systems without attractive boundaries, confirming again the universal nature of these finite-size corrections. Studying the disjoining pressure we found that the attractive boundaries have a stabilizing effect. This was noticed also in our previous work [3], however the curvature in the present case is very important. It makes the surface tension to be the predominant contribution to the disjoining pressure, as opposed to the slab geometry. Then, we conclude that the curvature has also a stabilizing effect on the system in comparison to the slab geometry in which the system can be unstable for low values of the adhesivity.

The study of the density profiles gives information about the structure of the system. As expected, there are some adsorbed charges on the boundary and these are screened by a positive layer of charge inside the system. We were able to check explicitly an electro-neutrality sum rule and a few relations that the adsorbed charge in the boundary satisfy.

It would be interesting to know what features of the present model are universal and which are not. A step toward answering this question can be obtained by studying another solvable model of Coulomb system, the one-component plasma. A preliminary study of this system was done in Ref. [15] and this will be the subject of a future paper.

Acknowledgments

The authors would like to thank the following agencies for their financial support: ECOS-Nord (France), COLCIENCIAS-ICFES-ICETEX (Colombia), Banco de la República (Colombia) and Fondo de Investigaciones de la Facultad de Ciencias de la Universidad de los Andes (Colombia).

-
- [1] M. L. Rosinberg, J. L. Lebowitz and L. Blum, A Solvable Model for Localized Adsorption in a Coulomb System, *J. Stat. Phys.* **44**:153–182 (1986).
 - [2] F. Cornu, Two-Dimensional Models for an Electrode with Adsorption Sites, *J. Stat. Phys.* **54**:681–706 (1989).
 - [3] G. Téllez and L. Merchán, Solvable Model for Electrolytic Soap Films: The Two-Dimensional Two-Component Plasma, *J. Stat. Phys.* **108**:495–525 (2002).
 - [4] L. Šamaj and I. Travěnek, Thermodynamic Properties of the Two-Dimensional Two-Component Plasma, *J. Stat. Phys.* **101**:713–730 (2000).
 - [5] L. Šamaj and B. Jancovici, Surface Tension of a Metal-Electrolyte Boundary: Exactly Solvable Model, *J. Stat. Phys.* **103**:717–735 (2001).
 - [6] L. Šamaj, Surface Tension of an Ideal Dielectric-Electrolyte Boundary: Exactly Solvable Model, *J. Stat. Phys.* **103**:737–752 (2001).
 - [7] M. Gaudin, L'isotherme critique d'un plasma sur réseau ($\beta = 2, d = 2, n = 2$), *J. Physique (France)* **46**:1027–1042 (1985).
 - [8] F. Cornu and B. Jancovici, On the Two-Dimensional Coulomb Gas, *J. Stat. Phys.* **49**:33–56 (1987).
 - [9] F. Cornu and B. Jancovici, The electrical double layer: A solvable model, *J. Chem. Phys.* **90**:2444–2452 (1989).
 - [10] P. J. Forrester, Density and correlation functions for the two-component plasma at $\Gamma = 2$ near a metal wall, *J. Chem. Phys.* **95**, 4545–4549 (1991).
 - [11] B. Jancovici, G. Manificat and C. Pisani, Coulomb Systems Seen as Critical Systems: Finite-Size Effects in Two Dimensions, *J. Stat. Phys.* **76**, 307–329 (1994).
 - [12] B. Jancovici and G. Téllez, Coulomb Systems Seen as Critical Systems: Ideal Conductor Boundaries, *J. Stat. Phys.* **82**, 609–632 (1996).
 - [13] B. Jancovici and L. Šamaj, Coulomb Systems with Ideal Dielectric Boundaries: Free Fermion Point and Universality, *J. Stat. Phys.* **104**, 753–775 (2001).

- [14] G. Téllez, Two-Dimensional Coulomb Systems in a Disk with Ideal Dielectric Boundaries, *J. Stat. Phys.* **104**, 945–970 (2001).
- [15] L. Merchán, *Two-dimensional Coulomb systems in a confined geometry subject to an attractive potential on the boundary*, Master Thesis (Universidad de los Andes, Bogotá, 2003).
- [16] P. J. Forrester, Surface Tension for the Two-Component Plasma at $\Gamma = 2$ near an Interface, *J. Stat. Phys.* **67**:433–448 (1992).
- [17] J. L. Cardy and I. Peschel, Finite-size dependence of the free energy in two-dimensional critical systems, *Nucl. Phys. B* **300**, [FS 22]:377–392 (1988).
- [18] J. L. Cardy, in *Fields, Strings and Critical Phenomena, Les Houches 1988*, E. Brézin and J. Zinn-Justin, eds. (North-Holland, Amsterdam, 1990).
- [19] M. Abramowitz and I. A. Stegun, *Handbook of Mathematical Functions* (National Bureau of Standards, Washington, D. C., 1964).
- [20] E. H. Hauge and P. C. Hemmer, *Phys. Norv.* **5**, 209 (1971).
- [21] S. Gradshteyn and I. M. Ryzhik, *Table of Integrals, Series, and Products* (Academic, New York, 1965).
- [22] G. N. Watson, *A treatise on the theory of Bessel functions* (Cambridge University Press, UK, 1922).
- [23] L. Merchán and G. Téllez, *Confined Coulomb systems with absorbing boundaries: The two-dimensional two-component plasma*, version 1, <http://arXiv.org/abs/cond-mat/0305514v1> (2003)
- [24] J. R. Henderson, in *Fundamentals of inhomogeneous fluids*, Chap. 2, D. Henderson, ed. (M. Dekker, New York, 1992).